# TECHNICAL RESEARCH REPORT

*Institute for Systems Research*

# Study of the Formation of Macro- and Micro-Cracks during Machining of Ceramics

*by G.M. Zhang, D.K. Anand, S. Ghosh, and W.F. Ko*

*The Institute for Systems Research is supported by the National Science Foundation Engineering Research Center Program (NSFD CD 8803012), Industry and the University*

TR 93-32r1

# Study of the Formation of Macro- and Micro-Cracks during Machining of Ceramics

G. M. Zhang, D. K. Anand, S. Ghosh, and W. F. Ko
Department of Mechanical Engineering and Institute for Systems Research
University of Maryland
College Park, MD 20742

This paper presents an experimental study on the formation of macro- and micro-cracks during machining of ceramic materials. In this study, Aluminum oxide ($Al_2O_3$) was the test material and polycrystalline diamond tipped carbide inserts were used. The cutting forces were recorded during each turning process and the surface finish was measured after machining. An environmental SEM was used to obtain high-magnification images of macro- and micro-cracks induced by machining. With the assistance of a computer-based vision system, quantification of fracture surfaces with respect to crack nucleation, growth, and cleavage was attempted. Results from this research provide an insight into the prevailing mechanisms of material removal during machining of ceramics, and suggest the development of microcrack-controlled machining technologies.

## 1. Introduction

The need for high-strength materials has led to the development of advanced ceramics. Advantages that ceramics have over other materials include superior heat resistance, wear resistance, and corrosion resistance. Increasing applications for ceramic materials are being found in industries such as aircraft, automobile, and micro-electronics.

Although most of the ceramic parts are manufactured to near net shape by pressing and sintering processes, precision machining is required to achieve a high degree of geometrical accuracy. Consequently, machining of ceramics has been a rapidly growing field. A traditional ceramics machining process is grinding where ceramic material is removed by the fine cutting edges of abrasives particles. In general, productivity of the grinding process is low, and micro-cracks are formed on and beneath the machined surface that often cause premature failure of ceramic components during service due to brittle fracture. With the ever increasing number of ceramic materials, new and innovative processing methods are needed to achieve cost reduction and quality assurance.

Many attempts have been made in this regard. As reported in (1), a "laser lathe" was developed where the dual beam principle was applied to remove ceramic materials in a molten form. However, the thermal damage induced on the surface and the sub-surface during laser machining is one of the drawbacks of the technique. Another processing method is abrasive jet machining, which uses a stream of high pressure fluid with abrasives insdes to pierce and wash ceramic materials away (2). But, the availability of the advanced equipment and the associated economic factors have limited its application on the shop floor. Recently, a new method, called "heat assisted machining," which integrates laser machining and grinding to remove ceramic materials in a ductile regime, is being developed. Product quality and productivity is expected to be significantly improved. However, with the wide selection of abrasive grains in the market to high levels of performance and dimensional accuracy, grinding is still widely used in machining ceramics (3).

This paper presents a research focused on basic understanding of the material removal mechanisms during machining of ceramic materials. Aluminum oxide ($Al_2O_3$) was the test material and Polycrystalline diamond tipped carbide inserts were used. All machining tests were performed on a CNC turning center. Cutting forces were recorded during machining and surface finish was measured after machining. An environmental SEM was used to examine both macro- and micro-cracks formed on the sample surfaces. With the assistance of a computer-based vision system, 3-dimensional images of the fracture surfaces were reconstructed and quantified with respect to the micro-crack formation during machining. Contour plots are used to characterize the size and shape of cracks and their orientation. Effects of three basic machining parameters, namely cutting speed, feed, and depth of cut, on the crack formation were investigated usinga factorial design technique. Results from this research provide an insight into the micromechanisms of material removal during machining of ceramics, and suggest the development of crack-controlled machining technologies.

## 2. Procedures of Experimental Investigation

Research results over the last few years have shown that material removal in machining ceramics is dominated by brittle fracture (4-6). Evans and Marshall investigated the cutting mechanisms of grinding ceramics. They pointed out that the cutting mechanisms (or wear mechanisms) are due to plastic flow and lateral cracking (7). They predicted a lateral fracture threshold loading limit. When the force developed during machining is below the loading threshold, plastic cutting occurs. On the other hand, lateral cracking occurs when the developed force is above the loading threshold. The interplay between the dynamic characteristics of a machining process and the micro-fracture mechanisms of the workpiece material at molecular level calls for a systematic study of the physics behind the material removal process during machining of ceramics. This research focuses on an experimental investigation, which consists of three major components:

1. Machining of ceramic material for sample preparation.
2. Profilometric measurements of machined surfaces.
3. SEM examinations of microstructural and fractographic feature of the material being machined.

## 2.1 Machining of Ceramic Material

Figure 1 shows the experimental setup for machining aluminum oxide ($Al_2O_3$). A CNC lathe was used. The machined $Al_2O_3$ is a cylindrical bar with initial diameter = 16 mm and length = 60 mm. The purity is 99.8% and the grain size is 10 - 12 μm. The material is a strong, dense recrystalized high-alumina ceramic material. Some material properties related to machining are listed below.

| | | |
|---|---|---|
| Hardness | 1100-1200 | kg/mm$^2$ |
| Modules of Elasticity | 380 | GPa |
| Compressive Strength | 3000 | MPa |
| Fracture Toughness | 4.0 | MPa*$\sqrt{m}$ |
| Melting Point | 2050 | °C |

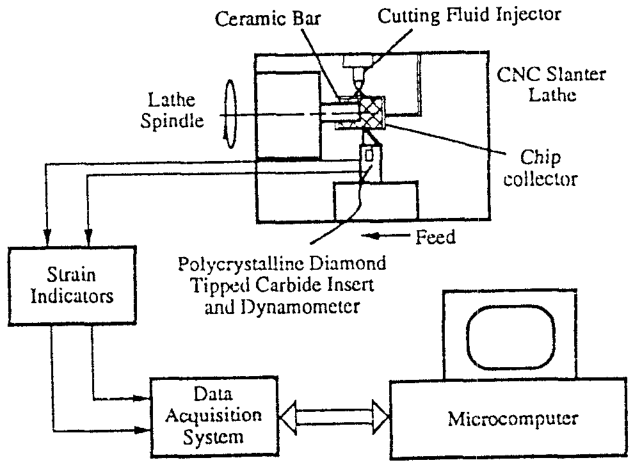

Figure 1 Experimental Setup for Machining Alumina

A dynamometer was attached to the toolpost and the tool holder was fixed on the dynamometer. During machining, polycrystalline diamond tipped carbide inserts, with nose radius 0.25 mm and -7 ° rake angle, were used to machine the alumina bars. In order to absorb the heat generated during machining, distilled water was used as cutting fluid during machining. Chips are collected in a funnel shaped device with a built-in filter to separate chip from the cutting fluid. The dynamometer measured the cutting force in both the cutting speed and feed directions. The data were recorded and stored in a PC-based data acquisition system.

For setting the machining conditions, or selecting feed, depth of cut, and cutting speed, a factorial design method with duplicates was used (8) Table 1 lists the eight combinations of the three machining parameter settings and the measured cutting force data in both the cutting speed and feed directions. For example, the row listed as Test 5 in Table 1 means:

(1) Three machining parameter settings are feed = 0.05 mm/rev, depth of cut = 0.77 mm, and cutting speed = 67m/min;
(2) The average measured cutting force component in the feed direction is 15.4 N (an average of two measurements, 13.9 N and 16.5 N), and the average measured cutting force component in the cutting speed direction is 6.5 N (an average of two measurements, 6.2 N and 6.7 N); and
(3) The measured roughness average value from the machined surface, $R_a$ = 2.30 µm.

## 2.2 Surface Finish Measurements

After machining, surface profiles were traced for the machined surfaces on a Talystep Stylus Instrument. In this research, the roughness average, $R_a$, was used as the characterization index for the finish quality evaluation. The eight measured $R_a$ values are listed in Table 1. The best finish quality, $R_a$ = 1.05 µm, was achieved at a combination of feed = 0.012 mm/rev, depth of cut = 0.26 mm, and cutting speed = 67 m/min. The worst finish quality, $R_a$ = 2.30 µm, was at a combination of feed = 0.05 mm/rev, depth of cut = 0.77 mm, and cutting speed = 11 m/min. These results are in agreement with the established metal machining theory. Figure 2 presents surface profiles along the feed direction and taken from four different samples. It is interesting to note that all the four patterns of height variation displayed in Fig. 2 are of random nature. No detectable effects of the tool nose radius and the tool motion pattern can be found with respect to the surface profile formation. However, these profiles display

Table 1 Machining Parameters Settings and Results

| Test No. | Parameters Settings | | | Force Measurements, N | | | | Resultant Force N | Surface Roughness, $R_a$ µm |
|---|---|---|---|---|---|---|---|---|---|
| | Feed mm/rev | Depth of Cut mm | Cutting Speed m/min. | Feed Force | | Tang. Force | | | |
| | | | | Run 1 | Run 2 | Run 1 | Run 2 | | |
| Test 1 | 0.012 | 0.772 | 67. | 8.36 | 8.47 | 3.56 | 3.60 | 9.14 | 1.35 |
| Test 2 | 0.012 | 0.772 | 11. | 22.46 | 22.68 | 4.98 | 4.93 | 23.11 | 1.92 |
| Test 3 | 0.012 | 0.264 | 67. | 3.83 | 3.71 | 2.16 | 2.05 | 4.32 | 1.05 |
| Test 4 | 0.012 | 0.264 | 11. | 3.24 | 5.03 | 1.47 | 1.99 | 4.48 | 1.15 |
| Test 5 | 0.051 | 0.772 | 67. | 13.94 | 16.49 | 6.16 | 6.67 | 16.51 | 2.17 |
| Test 6 | 0.051 | 0.772 | 11. | 21.34 | 23.99 | 8.72 | 8.75 | 24.29 | 2.30 |
| Test 7 | 0.051 | 0.264 | 67. | 4.24 | 3.93 | 3.08 | 2.91 | 5.07 | 1.51 |
| Test 8 | 0.051 | 0.264 | 11. | 5.76 | 5.14 | 2.61 | 2.20 | 5.96 | 1.70 |

several deep valleys along the feed direction. The deepest valleys are found in the case of high feed and large depth of cut (Fig. 2d). These narrow and deep valleys suggest occurrence of brittle fracture during the chip formation.

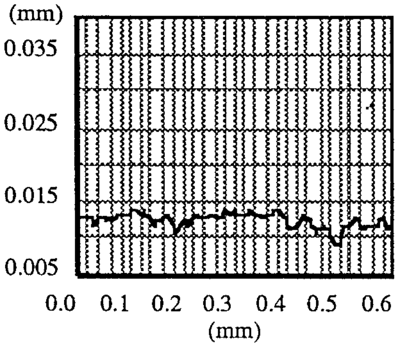

Ra = 1.05 μm

(a) Test 3: f=0.012 mm/rev, d = 0.264 mm, v= 67 m/min

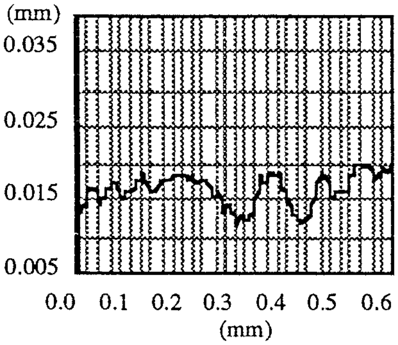

Ra = 1.35 μm

(b) Test 1: f=0.012 mm/rev, d = 0.772 mm, v= 67 m/min

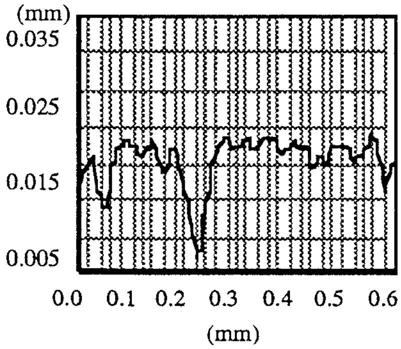

Ra = 1.70 μm

(c) Test 8: f=0.051 mm/rev, d = 0.264 mm, v= 11 m/min

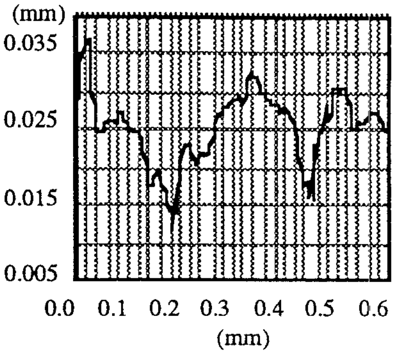

Ra = 2.30 μm

(d) Test 6: f=0.051 mm/rev, d = 0.772 mm, v= 11 m/min

Figure 2 Surface Profiles Measured from the Machine Surface

### 2.3 SEM Examination

To understand the process of chip formation during machining and identify the relationship between the fracture mode and the microstructure of the materail, a detailed examination and analysis of the fracture surface is required. In this research, an environmental scanning electron microscope (ESEM) was used to obtain high-magnification images that provide details about the geometry of the formed chips and the topography of the machined surfaces. Another advantage of using ESEM is that no conductive coating is required as in the case of ordinary SEM. This allows a direct identification of macro- and micro-cracks induced by machining without the influence of applied coating.

Figure 3 presents a set of electron micrographs of the chips collected during machining. Figure 4 presents a set of micrographs of the surfaces machined under the eight combinations of depth of cut, feed, and cutting speed settings at two levels.

## 3. Analysis of Experimental Results

The basic philosophy applied for data analysis is first to identify if there are similarities between the machining of ceramic materials and the machining of metals. Afterwards, focus will be given to analyzing new and important findings. It is expected that there exist significant differences in the micromechanisms of material removal between the two types of machining process.

## 3.1 Cutting Force Generated during Machining

Following observations are made by examining the cutting force results listed in Table 1:

1. The cutting force produced during machining is proportional to the cutting area. The small cutting forces, such as 4.32 N and 4.48 N, are associated with the combinations of low feed and depth of cut settings, and the largest cutting forces, such as 24.3 N and 23.1 N, with the combinations of high feed and depth of cut settings. This observation follows the law of material strength, i.e., force is proportional to the applied area at a given stress level, or at a given loading threshold.

2. As a first approximation, the unit cutting force, calculated as a ratio of the measured cutting force to the cutting area, ranges from 650 N/mm$^2$ to 2500 N/mm$^2$. The low limit of the unit cutting force happened during machining at a high cutting speed setting, a phenomenon that could be interpreted as the effect of high temperature on the material removal. However, such a wide variation of unit cutting force can only be contributed to the fact that the fracture strength of a brittle material fluctuates. The fluctuation can be as much as an order of magnitude (5). In fact, this characteristic indicates that ceramic materials can be removed at a low unit cutting force if the machining condition is preferred, pointing out great promise to search new and innovative machining technologies.

3. The magnitude of the tangential cutting force component is much smaller than that of the cutting force component along the feed direction, a phenomenon just opposite to what has been observed during the machining of metals where the magnitude of the tangential force is much larger than that of the feed force.

## 3.2 Mechanisms of Material Removal

The analysis presented in this section includes a detailed examination and analysis on fracture mechanisms for clarification of the role of the microstructure, or understanding the metallurgical factors that control the material removal process. The analysis is first divided into two parts for examining the chip formation and surface topography formation, respectively. Then we combine the results from these analyses and propose a model to describe the mechanisms of material removals including the chip formation process. Special efforts are made to illustrate a developed computer vision system for visualizing and quantifying the fracture surface formed during machining.

### 3.2.1 Mechanisms of Chip Formation

Information on the chip formation mechanisms can be obtained through the examination of the four micrographs of chips shown in Fig. 3:

1. The chip fragments shown in Fig. 3a and Fig. 3b were formed during two machining processes with depth of cut settings at 0.77 mm and 0.26 mm, respectively. It is not surprising to conclude that a high material removal process, such as the one with a large depth of cut, will produce large chip fragments. However, the size of chip fragments formed during a single machining process varies significantly. For example, the chip fragments shown in Fig. 3b are significantly different in size. This phenomenon indicates that special attention must be paid to the investigation of chip formation during machining of ceramic materials.

2. The two chip fragments shown in Fig. 3d were taken at a high magnification. They represent two types of chip observed in this experimental study. The unique feature among the two types of chips is their lateral surfaces, which are formed by brittle fracture. This feature indicates that the chip formation during machining is a macro-scale fracture process, or cleavage fracture

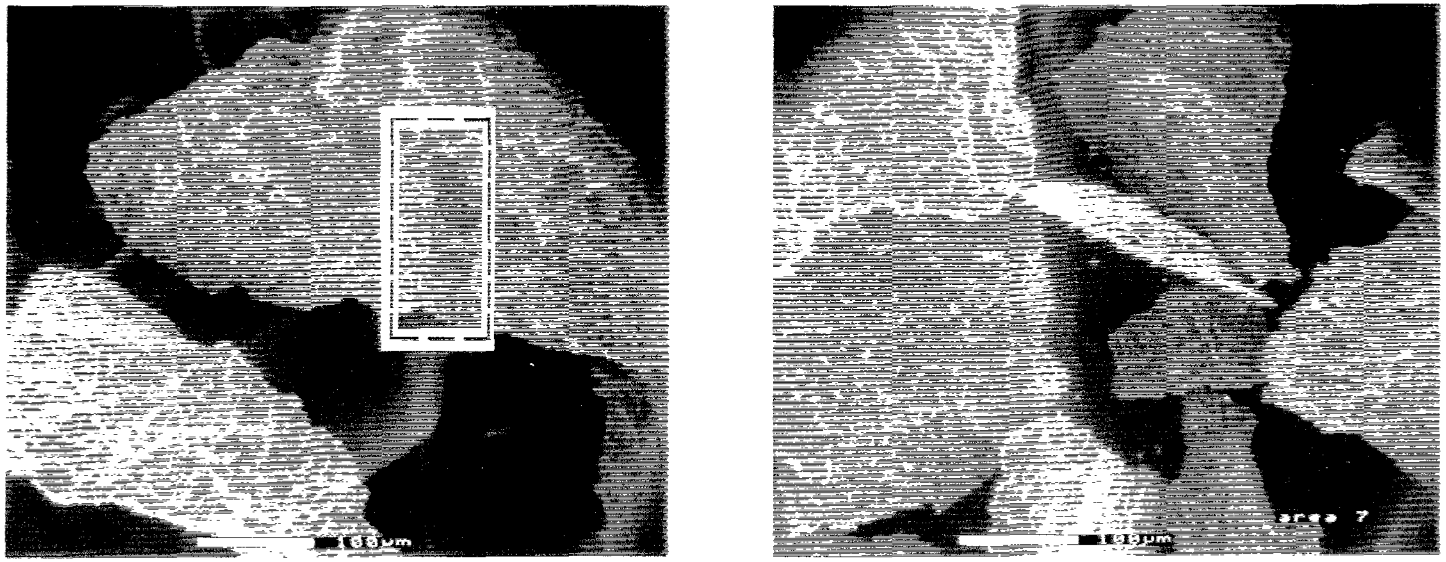
100µm
100µm
area 7

(a) Test 6 f=0.05 mm/rev, d=0.77 mm, v=11 m/min

(b) Test 8 f=0.05 mm/rev, d=0.26 mm, v=11 m/min

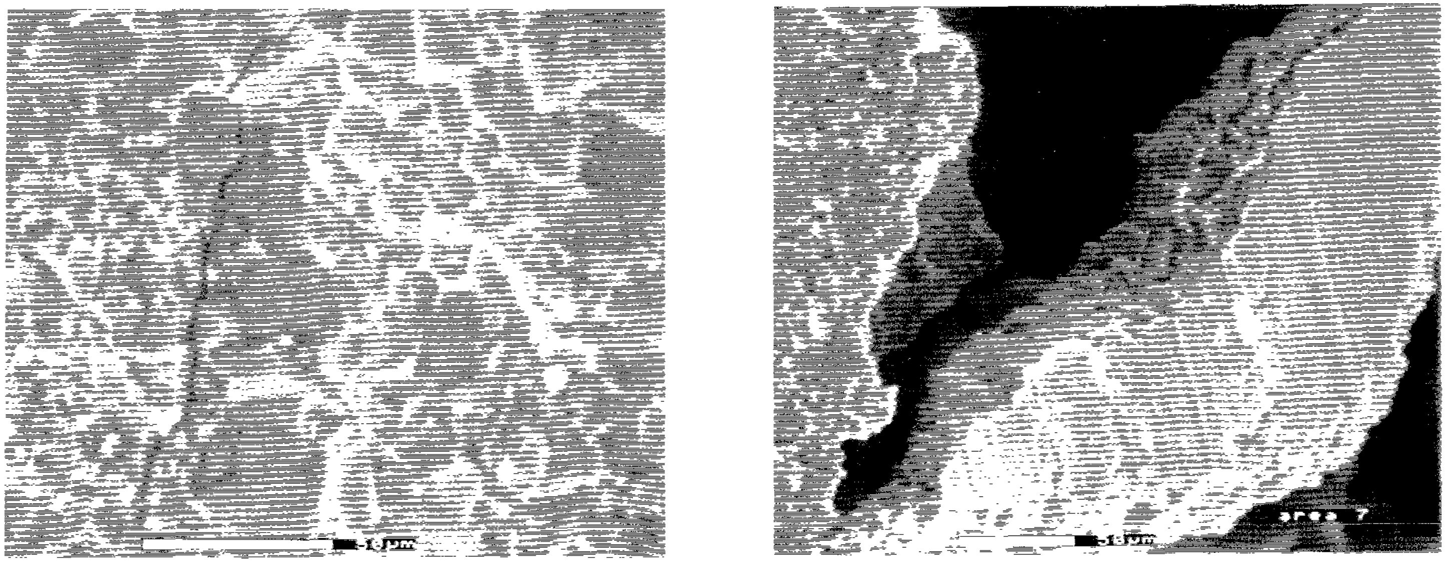
10µm
10µm
area 7

(c) Crack Trapped in the Cleavaged Chip (Test 6)

(d) Machined Chip with Plowing Marks (Test 6)

Figure 3 SEM Micrographs of the Chips Formed during Machining

Feed = 0.012 mm/rev.

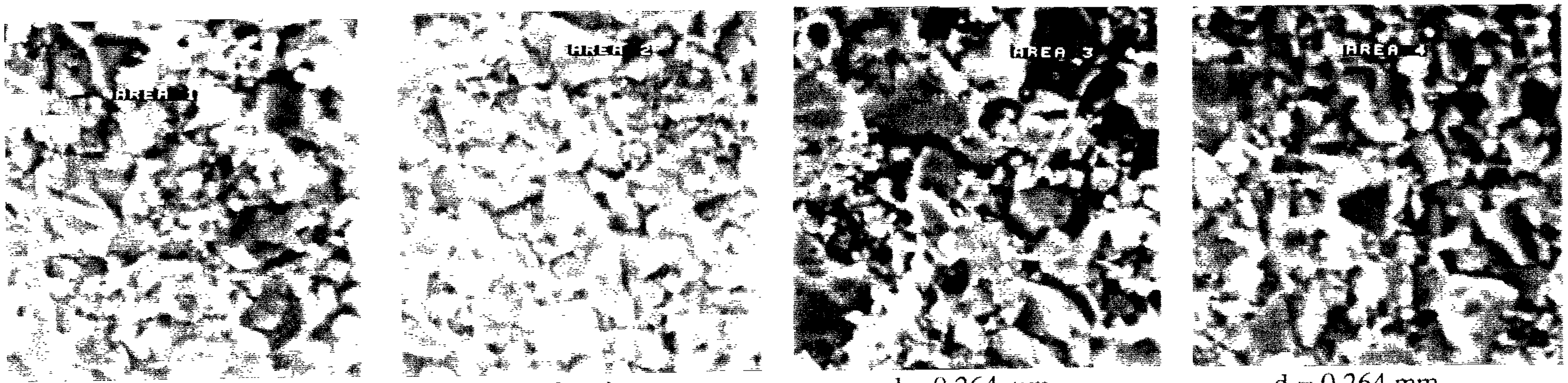
AREA 1
AREA 2
AREA 3
AREA 4

(a) d = 0.772 mm
v = 67. m/min.

(b) d = 0.772 mm
v = 11. m/min.

(c) d = 0.264 mm
v = 67. m/min.

(d) d = 0.264 mm
v = 11. m/min.

Feed = 0.051 mm/rev.

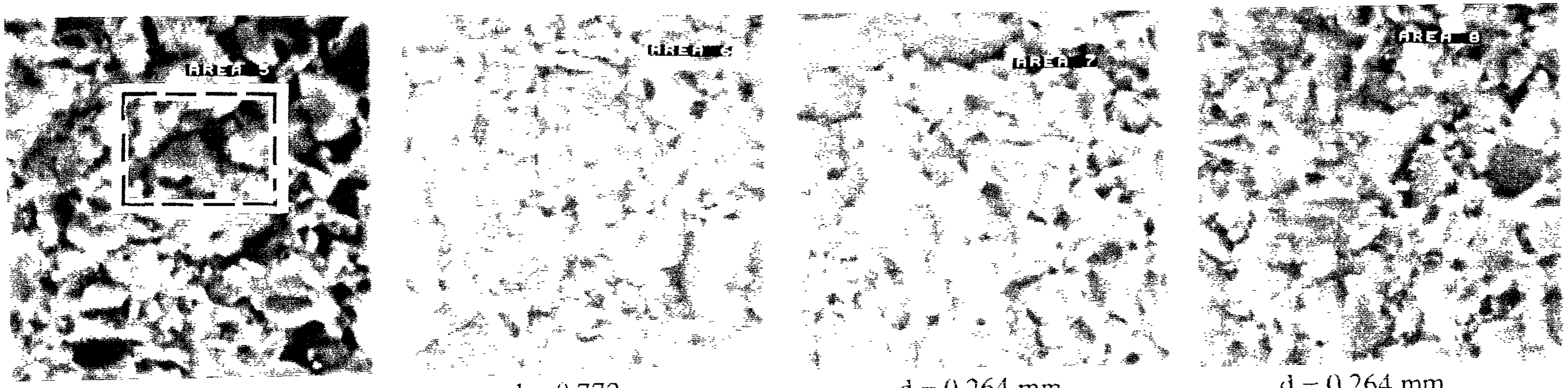
AREA 5
AREA 6
AREA 7
AREA 8

(e) d = 0.772 mm
v = 67. m/min.

(f) d = 0.772 mm
v = 11. m/min.

(g) d = 0.264 mm
v = 67. m/min.

(h) d = 0.264 mm
v = 11. m/min.

Figure 4 SEM Micrographs of the Machined Surfaces under the 8 Combinations ( x 500 )

mode. However, there exists a unique difference between these two types of chip. The chip on the right side of the figure has a smooth flat surface. The parallel lines, or the plowing marks, on the smooth surface resemble the chip flow over the rake face of a cutting tool, a phonomenon routinely observed during machining of metals. Note that this chip was formed under a machining condition where the temperature measured in the cutting zone was about 750$^{\circ}$C. This suggests that formation of this type of chip could start from plastic deformation in the cutting zone, then progress into plastic flow over the rake face, and end with separation from the machined part due to fracture. This suggestion can be interpreted as the existence of deformation mode in a fracture process for brittle materials (5, 8). Research in the future direction should pursue applying the elastic-plastic fracture mechanics to characterize the crack tip field in the chip formation process. Figure 5 illustrates the proposed formation process of the two types of chip, namely, the machined chip and the fractured chip during machining. The fractured chip is defined as those chip fragments formed without direct contact to, or flow over, the tool rake face. This may provide an explanation to the random nature of the height variation pattern observed in taking surface profiles from the machined surface.

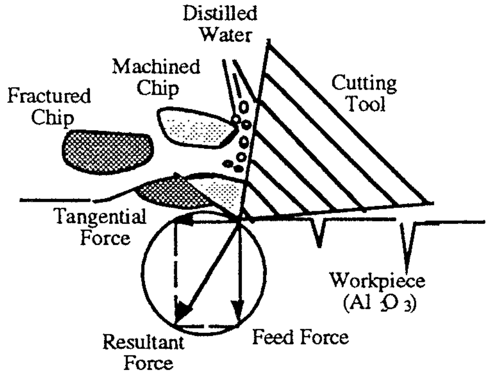

Figure 5 Two Types of Chip Formed during Machining of Alumina

3. The micrograph at a high magnification shown in Fig. 3c depicts the intergranular fracture developed within a fractured type of chip formed during machining. The location of the crack with respect to the chip as a whole is marked in Fig. 3a. It shows that the crack is about 5 $\mu$m in width and 120 $\mu$m in length. It is intersting to note that this crack was trapped when a fractured chip was formed; indicating that the formation of fractured chip fragments is due to the catastrophic failure of the ceramic material under high stresses (above the loading threshold), developed during machining.

### 3.2.2 Mechanisms of Surface Topography Formation

One of the ultimate objectives of machining engineering ceramics is to achieve a high degree of the geometrical accuracy of a designed part. The topography formed on a machined surface plays a key role in this regard. Based on the previous discussion, the machined surface is an assemblage of fracture surfaces left by the chip formation. Reliability of a machined part during its service period is directly related to the status of macro- and micro-cracks formed on the machined surface as well as the region just beneath the machined surface. A new approach, which integrates profilometry, microscopic analysis and image processing, is developed to investigate the mechanisms of surface topography formation (9).

1. Macro- and microscopic examination of the fracture surface. The eight micrographs shown in Fig. 4 are the images taken from the surfaces machined under the eight machining conditions with a magnification of 500. The intergranular fracture along the grain boundaries can be clearly identified on these machined surfaces, indicating their preferred, river-like crack paths, as depicted in Fig. 4. An important observation is that almost all of the intergranular cracks initiated at triple point junctions (intersections of the grain boundaries) and dislocation pile-ups at the grain boundaries. Figure 6 is a micrography of a chip fragment collected during machining. A magnification of 4,500 is used to reveal both microstructural and fractographic

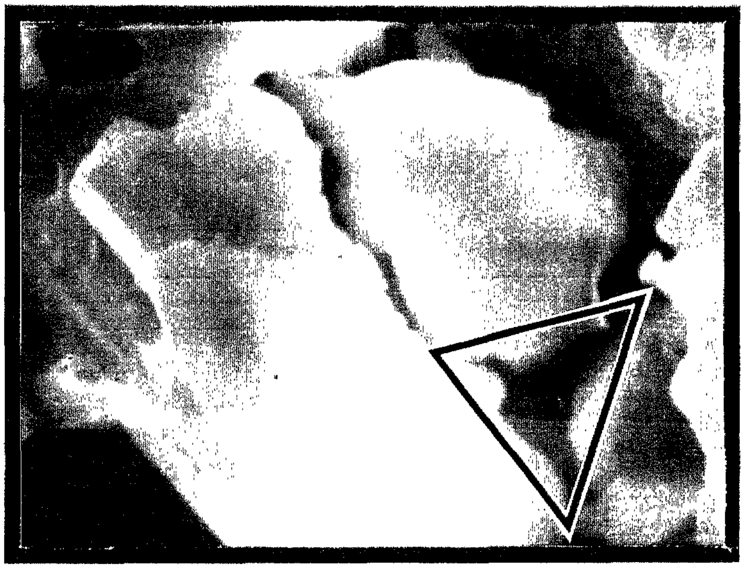

Figure 6 Microstructural and Fractographic feature around a Single Grain (A Triple Point Junction Is Indicated)

feature around a single grain. The picture depicts the three pairs of contacting points between the neighboring grains. It is very likely that the cutting force induces local residual tensile stresses at these triple points during machining. In combination with stresses from deformation generated within the grains due to the cutting action, crack nucleation is initiated at these locations. As the machining process goes on, the progressive development of grain boundary microcracking leads to crack growth, or propagation. Figure 6 also illustrates the cleavages due to microcracking at the triple point junctions. The progression of intergranular cracks causes an entire grain to dislodge from the machining area, leading to intergranular fracture or cleavage fracture. The process of grain dislodging forms micro-cracks, and then macro-cracks, and finally, the topography of a machined surface.

2. Profilometric examination. By examining Fig. 2 and Table 1 jointedly, a small Peak-to-Valley value is associated with a machining process with a small cutting force. It indicates that most of the crack initiation, growth, and cleavage were confined with a very limited local areas, or "short-crack" regions (5), when the cutting force was rather small. As these "short-cracks" extended, the toughness of alumina built up and resisted extension of these developed cracks. Figure 7 illustrates a steadily increasing toughness with expanding crack size for alumina (5). On the other hand, the profile with a large Peak-to-Valley value is associated with a machining process generating a large cutting force. This indicates that the induced local residual tensile stresses exceeded a critical value, but the toughness keeps at a constant level because the crack length has reached a critical value, say 10 µm illustrated in Fig. 7 for alumina. Under such circumstances, accelerated crack propagation will lead to the occurrence of catastrophic failure of alumina. During machining, this could imply the increase of formed fractured chip fragments. An excessive amount of fractured chip fragments could introduce large irregularities on the

machined surface, as illustrated in Fig. 2d.

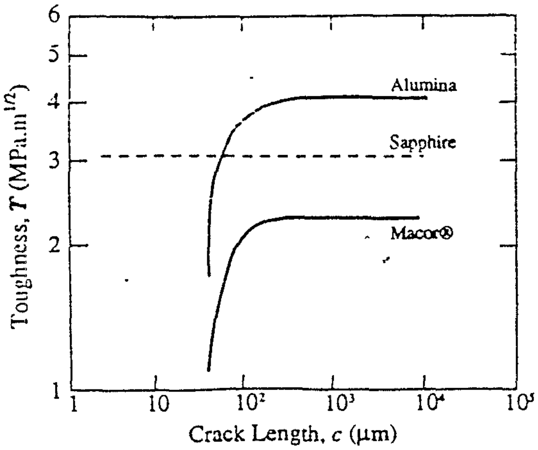

Figure 7 Fracture Toughness as a Function of Crack Length (5)

3. Stereophotogrammetric examination through image processing. Stereoscopy offers a direct and nondestructive procedure for determining the elevation of a fracture surface at selected regions (10-12). In this research, a software package, which integrates image processing, profilometry, and computer graphics, was developed to visualize the surface topography formed during machining, display patterns of crack propagation, and quantify the size and shape of intergranular and transgranular cracks from the ESEM micrographs. Figure 8 presents a visualized surface topography in three-dimensional space and an associated contour map. The corresponding area of the surface topogarphy is marked in the micrograph shown in Fig. 4e(area 5). The reconstructed fracture surface topography vividly depicts the surface texture formation during machining. It visualizes the appearance of surface cracks and quantifies the relative positions between the surface roughness and the surface cracks. For example, the distance 4.2 μm marked in Fig. 8a, obtained through calibration using the profilometric measurements, provides a valuable information for post-machining, such as grinding and polishing, as well as reliability assessment of the machined parts. By examining the deduced contour map shown in Fig. 8b where the interval between the contour lines is 0.5 μm. The numbers shown outside the frame are the heights of the location, the

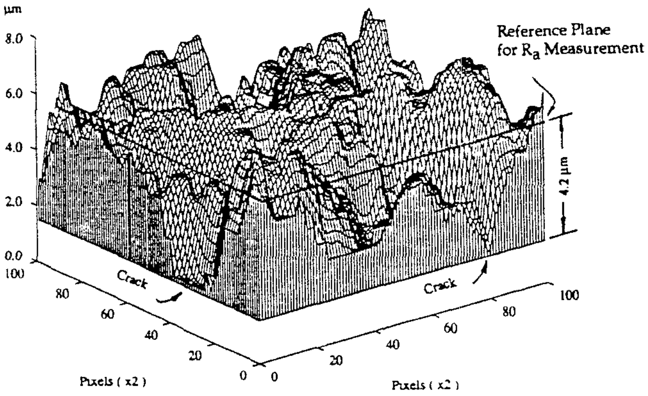
μm
8.0
6.0
4.0
2.0
0.0
Reference Plane for $R_a$ Measurement
4.2 μm
Crack
Crack
100
80
60
40
20
0
Pixels ( x2 )
Pixels ( x2 )

(a) Visualization of Surface Topography and Crack Indications

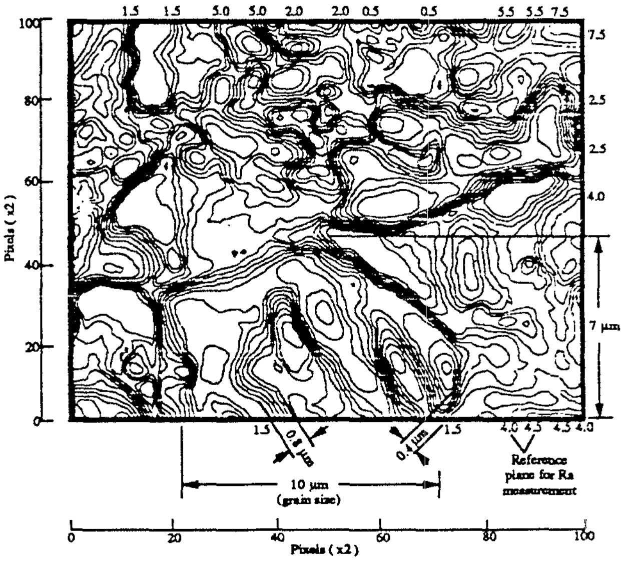
1.5 1.5 5.0 5.0 2.0 2.0 0.5 0.5 5.5 5.5 7.5
7.5
2.5
2.5
4.0
7 μm
Pixels ( x2 )
100
80
60
40
20
0
1.5
0.8 μm
0.4 μm
1.5
4.0 4.5 4.5 4.0
Reference plane for Ra measurement
10 μm (grain size)
0
20
40
60
80
100
Pixels ( x2 )

(b) Contour Map for Quantifying the Formed Cracks

Figure 8 Fracture Surface Reconstruction and Crack Closure

lowest point of the surface topography being taken as 0.0 µm. On the other hand, the pixel number, as illustrated in Figs, 8a and 8b, provides a scale for calculating dimensions in a horizontal plane. By adding the width between two contour lines, a quantitative information about the size and shape of a crack can be estimated. For example, the width marked as 0.4 µm in Fig. 8b covers 6 contour lines. The information provides the size of a V-shape crack having an angle of $7.6^{o}$ with its vertex 4.2 µm away from the reference plane for $R_a$ measurements. It is interesting to note that the contour map could assist us in identifying transgranular cracks. For example, the boundaries of a grain sized 10 µm can be identified on the map, as shown in Fig. 8b. Within the grain, a crack path is also identified. It is marked 0.8 µm. If further investigation on this spot is pursued, we might be able to have information about transgranular cracks developed by machining. The principal objective of modern quantitative fractography is to express the geometric characteristics of the features on the fracture surface in quantitative terms. The stereophotogrammetric examination through image processing developed in this research may provide a powerful tool to establish the quantitative relationships between the crack formation and machining conditions.

## 3.3 Material Removal Mechanisms during Machining

From the above discussion, as a material removal process, machining of ceramic materials shares certain common characteristics with what we have observed from machining of metals. Both machining processes involve cutting force generation, chip formation, and surface topographical generation. However, machining of ceramic materials possesses unique characteristics. Based on our experimental work, we present a model to describe the material removal process with emphasis on the relationships between the macroscopic and microscopice fracture behaviors. Figure 9 illustrates the five essential stages in this basic physical process:

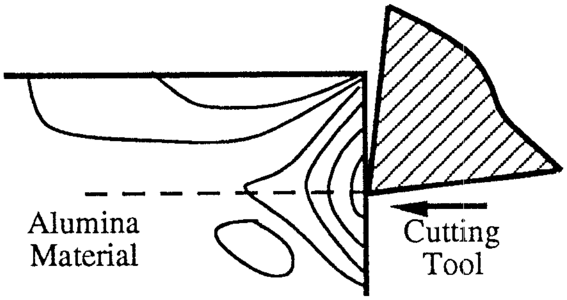

(a) Dynamic Loading and Induced Stress Field

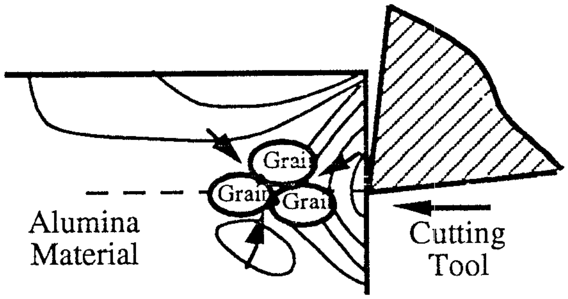

(b) Crack Initiation

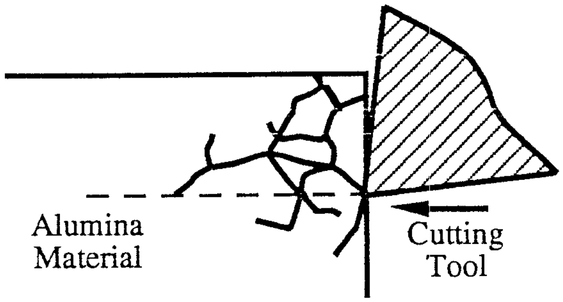

(c) Crack Propagation

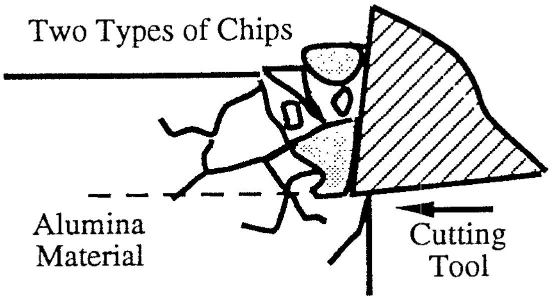

(d) Chip Formation

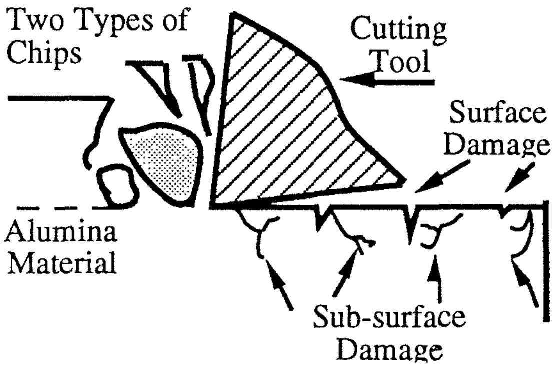

(e) Formation of Surface and Sub-surface Damage

Figure 9 Five Essential Stages in the Material Removal

1. Dynamic Loading. When a machining process starts, the tool approaches to the part material. At the instant when the tool touches the part material, the impact between them induces stresses in the material and a stress field is formed (Fig. 9a).

2. Crack Initiation. When subjected to the induced stresses, crack nucleation begins immediately. Their sites are locations of stress singularities where high internal tensile stresses build up. These locations can be triple-point junctions, dislocation pile-ups at grain boundaries, and second-phase particles. All of these flaws could initiate micro-cracks (Fig. 9b).

3. Crack Propagation. As the machining process goes on and stresses continue to develop in the material, the formed microcracks grow in the material immediately surrounding them. Both intergranular and trangranular cracks are developed and advanced obstacles are encountered (Fig. 9c).

4. Chip Formation. The process of crack propagation is terminated when more micro-cracks propagate and produce unstable fracture. The material separated by fracture can be in a position either contacting with the rake face of the cutting tool or away from the cutting zone, depending on the pattern of crack propagation. Consequently, two types of chip will be formed. The type of machined chip (shadow areas) represents the fractured material directly under the tool action and also subjected to the temperature influence. On the other hand, the type of fractured chip depends on the pattern of crack propagation, which is governed by the material microstructure (Fig. 9d).

5. Formation of Surface and Sub-surface Damage. Due to brittle fracture, chip fragments are formed during machining. At the same time, surface texture is formed on the machined surface with cracks because brittle fracture. These cracks are called surface damage and, in general, unavoidable during machining of ceramic materilas. In addition, the residual effects of brittle facture near the surface layer bury numerous micro-cracks to a certain depth, leading to sub-surface damage (Fig. 9e).

### 3.4 Development of Crack-controlled Machining Technologies

Based on the comprehensive understanding of material removal mechanisms, we should have gained guidelines for developing new and innovative machining technologies to control the crack formation. The following suggestions are made in this regard.

1. Control of Microstructure of Ceramic Material. It has been recognized that machinability can be significantly improved by controlling microstructure of metals through heat treatment. The same philosophy applies to the machining of ceramic materials as well. The microstructure of ceramic materials is central to strength and toughness properties. By controlling the size and shape of individual grains, or the volume fraction of incorporated second phases, we may be able to balance the need for avoiding structure failure from design point of view and the need for degrading short-crack toughness from the viewpoint of improving machinability. A typical example would be the development of Dicor/MGC, a glass-ceramic material designed for use in dental restorations (14). The material has a unique microstructure consisting of mica flakes of approximately 70 volume percent dispersed in a non-

porous glass matrix. The cleavage along the literal planes of mica flakes functions as stress concentration, a situation similar to the stress concentration around the inclusions in free-machining steels, offering an excellent machinability.

2. Control of Machining Parameters. It is certain that the tool geometry will play a key role in determining the distribution of induced stresses in the material being machined. By limiting the volumetric ratio of fractured chip to machined chip, we may be able to manage surface and sub-surface damage. The ductile region grinding is a typical example of keeping at a low level or eliminating the formation of fractured chip during machining. Proper selections of the three cutting parameters (feed, depth of cut, and cutting speed) may render an optimal machining performance possible. In the study of environmental effects on fracture mechanics, it has been well recognized that stress-corrosion cracking causes intergranular or cleavage separation by a loss of cohesion (15). Therefore, use of cutting fluids can improve machining efficiency. In fact, chemical-assisted machining has been studied intensively, showing great promise for crack-controlled machining (16-17).

3. New Processing Methods. Laser-based heat assisted machining is being developed. By controlling the temperature of the cutting zone, an increase of pre-fracture plastic deformation could reduce brittle fracture significantly, leading to a full control of machining process. On the other hand, crack arrest through post-processing would be a typical example to improve surface quality after machining.

## 4. Conclusions

In this research, a fundamental study related to machining of alumina is conducted. It consists of cutting force measurement, assessment of surface finish quality, and analysis of micromechanisms of material removal during machining. The results are summarized as follows.

1. Machining of ceramic materials is characterized by crack initiation and propagation, leading to chip formation. There are two types of chip, i.e., machined chip and fractured chip. nd cleavage fracture are the three key elements in the machining process. A model is proposed to describe the material removal process.

2. By integrating image processing, profilometry and computer graphics, a computer-based vision system is developed for expressing the geometric characteristics of features on the fracture surface through three-dimensional visualization and contour mapping.

3. Collaboration between shop floor machinists and material processing engineers is needed. to 1). optimize ceramic microstructures, that provide required resistance to the initiation and propagation of brittle cracks while maintaining an acceptable machinability; and 2). develop new and innovative machining technologies for effectively controlling the crack formation during machining.

## Acknowledgements

The authors acknowledge the support of the University of Maryland Research Board, the Department of Mechanical Engineering, and the Institute for Systems Research at the University of Maryland under Engineering Research Centers Program: NSFD CDF 8803012. Special thanks are due Mr. Myron E. Taylor, Directior of the Central Facility for Microanalysis, who provided valuable assistance in conducting the SEM study. The technical discussions with Dr. Brain Lawn of the National Institute of Standards and Technology, and Dr. Isabel Illoyd and Dr. James Dally of the University of Maryland provided many insights of this research. The assistance from Mr. Doug Beale and Mr. Don DeVoe during the course of this work is also appreciated.

## References

1. G. Chryssolouris, J. Bredt, S. Kordas, and E. Wilson, "Theoretical Aspects of a Laser Machine Tool," ASME Winter Annual Meeting Proceedings, PED 20, pp. 177-190, December 1986.

2. M. Mazurkiewicz, "Understanding Abrasive Waterjet Performance,"

Machining Technology, Vol. 2, No.1, pp. 1-3, 1991.

3. K. Subramanian, S. Ramanath, and Y. O. Matsuda, "Precision Production Grinding of Fine Ceramics," Proceedings of the First International Conference on Manufacturing Technology, Chiba, Japan, 1990.

4. R. C. Bates, "Micromechanical Modeling for Prediction of Lower Shelf, Transition Region, and Upper Shelf Fracture Properties," Part 3, in Fracture Mechanics: microstructure and micromechanisms," Edited by Nair, et al, ASM International, pp. 131-168, 1989.

5. B. R. Lawn, "Fracture of Brittle Solids," Second Edition, Cambridge University Press, Cambridge, in press.

6. J. Cagnoux, and A. Cosculluela, "Influence of Grain Size on Triaxial Dynamic Behavior of Alumina," Part 6 in Dynamic Failure of Materials: Theory, Experiments, and Numbers," Eds. H. Rossmanith, and A. Rosakis, Elsevier Applied Science, pp. 73-84, 1991.

7. A. G. Evan, and D. B. Marchall, "Wear Mechanisms in Ceramics," In Fundamentals of Friction and Wear, Ed. D. A. Rigney, Metals Park, Ohio, American Society of Metals, pp. 439-452, 1980,.

8. G. Box, W. Hunter, and J. Hunter, "Statistics for Experimenters, An Introduction to Design, Data Analysis, and Model Building," John Wiley & Sons, Inc., 1978.

9. J. Landes, and R. Herrera, "Micromechanisms of Elastic/Plastic Fracture Toughness," Part 4, in "Fracture Mechanics: microstructure and micromechanisms," Edited by Nair, et al, ASM International, pp. 111-130, 1989.

10. K. Komai, and M. Noguchi, "Fracture Surface Reconstruction Technique and Crack Closure," Part 5, in "Fractography", Edited by Koterazawa, et al., Elsevier Applied Science, pp. 161-186, 1990.

11. E. E. Underwood, "Recent Advances in Quantitative Fractography," Part 2, in Fracture Mechanics: microstructure and micromechanisms," Edited by Nair, et al, ASM International, pp. 87-109, 1989.

12. E. E. Underwood, "Quantitative Fractography", Chapter 8, in Applied Metallography, G. F. Vander Voort, Ed., Van Nostrand Reinhold, pp. 101-122, 1986.

13. J. E. Hilliard, Quantitative Analysis of Scanning Electron Micrographs," Journal of Microscience, 95, Part 1, pp. 45-58, 1972.

14. D. Grossman, "Structure and Physical Properties of Dicor/MGC Glass-Ceramic," Proceedings of the 1991 International Symposium on Computer Restorations, Regensdort-Zurich, Switzerland, pp. 103-115, 1991.

15. W. Gerberich, "The Micromechanics and Kinetics of Environmentally Induced Fractures," Part 3, in "Fracture Mechanics: microstructure and micromechanicsms," Edited by Nair, et al, ASM International, pp. 201-208, 1989.

16. G. Zhang, T. Hwang, D. Anand, and S. Jahanmir, "Tribological Interaction in Machining Aluminum Oxide Ceramics," Proceedings of the Navy Tribology Workshop, Annapolis, Maryland, May 11-13, pp. 9-13, 1992.

17. G.M. Zhang, T.W. Hwang, and D.K. Anand, "Chemo-Mechanical Effects on the Efficiency of Machining Ceramics," Proceedings of 1993 National Science Foundation Design and Manufacturing Systems Conference, Charlotte, NC, January, pp. 421-428, 1993.